

The influence of facies heterogeneity on the doublet performance in low-enthalpy geothermal sedimentary reservoirs

Crooijmans, R. A.; Willems, C. J L; Maghami Nick, H.; Bruhn, D. F.

DOI

[10.1016/j.geothermics.2016.06.004](https://doi.org/10.1016/j.geothermics.2016.06.004)

Publication date

2016

Document Version

Accepted author manuscript

Published in

Geothermics

Citation (APA)

Crooijmans, R. A., Willems, C. J. L., Maghami Nick, H., & Bruhn, D. F. (2016). The influence of facies heterogeneity on the doublet performance in low-enthalpy geothermal sedimentary reservoirs. *Geothermics*, 64, 209-219. <https://doi.org/10.1016/j.geothermics.2016.06.004>

Important note

To cite this publication, please use the final published version (if applicable). Please check the document version above.

Copyright

Other than for strictly personal use, it is not permitted to download, forward or distribute the text or part of it, without the consent of the author(s) and/or copyright holder(s), unless the work is under an open content license such as Creative Commons.

Takedown policy

Please contact us and provide details if you believe this document breaches copyrights. We will remove access to the work immediately and investigate your claim.

The influence of facies heterogeneity on the doublet performance in low-enthalpy geothermal sedimentary reservoirs

R.A. Crooijmans ^a, C.J.L. Willems ^a, H.M. Nick ^{a,b}, D.F. Bruhn ^{a,c}

^a *Faculty of Civil Engineering and Geosciences, Delft University of Technology, The Netherlands*

^b *The Danish Hydrocarbon Research and Technology Centre, Technical University of Denmark*

^c *Helmholtz Centre Potsdam - GFZ German Research Centre for Geosciences*

Keywords: non-isothermal flow, variable fluid properties, heterogeneity, geothermal, doublet, sedimentary formation, net to gross ratio.

*rogiercrooijmans@hotmail.com

1 **Abstract**

2 A three-dimensional model is used to study the influence of facies heterogeneity
3 on energy production under different operational conditions of low-enthalpy
4 geothermal doublet systems. Process-based facies modelling is utilised for
5 the Nieuwerkerk sedimentary formation in the West Netherlands Basin to
6 construct realistic reservoir models honouring geological heterogeneity. A
7 finite element based reservoir simulator is used to model the fluid flow and
8 heat transfer over time. A series of simulations is carried out to examine the
9 effects of reservoir heterogeneity (Net-to-Gross ratio, N/G) on the life time
10 and the energy recovery rate for different discharge rates and the production
11 temperature (T_{min}) above which the doublet is working. With respect to
12 the results, we propose a design model to estimate the life time and energy
13 recovery rate of the geothermal doublet. The life time is estimated as a
14 function of N/G, T_{min} and discharge rate, while the design model for the
15 energy recovery rate is only a function of N/G and T_{min} . Both life time
16 and recovery show a positive relation with an increasing N/G. Further our
17 results suggest that neglecting details of process-based facies modelling may
18 lead to significant errors in predicting the life time of low-enthalpy geothermal
19 systems for N/G values below 70%.

20 **1. Introduction**

21 Geothermal energy production from deep geological formations has been
22 growing in the Netherlands since the first doublets were realised in 2007(van
23 Heekeren, 2015). The main targets are sedimentary fluvial reservoirs at
24 depths between 2 and 2.5 km with a temperature between 70 and 90 °C

25 (Bonté et al., 2012). These are so-called low-enthalpy reservoirs, which
26 are mainly used for heating of buildings in the horticultural sector. The
27 sedimentary fluvial reservoirs have different characteristics from conventional
28 geothermal in magmatic settings. Such characteristics are, for example,
29 porosity, initial temperature, permeability and heat capacity that lead to
30 different geothermal performance indicators such as the life time of the
31 doublet (how long the doublet can produce economically), recovery (produced
32 energy compared to the total amount of available energy) and the daily
33 energy production. The performance indicators together with the operational
34 costs determine the profitability of the geothermal system. The focus of this
35 study is on the performance of such a system where the life time and the
36 recovery are dependent on both human and physical controlled parameters.

37 Saeid et al. (2015) suggest that the most influencing human controlled
38 parameter is the discharge of the wells. Not surprisingly, the larger the
39 discharge the faster the cooling of the reservoir is noticeable in the production
40 fluid (i.e. the earlier the arrival of the cold water front). Other important
41 human controlled parameters are injection temperature and well spacing.
42 The larger the difference in temperature between the produced and injected
43 fluid, the more energy is extracted from the reservoir; and the closer the wells
44 the faster the cold water reaches the production well.

45 The main physical controlled parameters are porosity, salinity of the pore
46 fluid, initial reservoir temperature (Saeid et al., 2015), reservoir thickness and
47 the thickness of shale layers in between the reservoir bodies (Poulsen et al.,
48 2015). The salinity of the pore fluid and the initial reservoir temperature
49 can be assumed constant at reservoir scale. Porosity is, however, strongly

50 heterogeneous and dependent on the facies. Facies are geological bodies
51 formed by sedimentological processes, which are dependent on the paleo-river
52 behaviour. This makes the distribution of the facies unique for each river
53 deposit. The facies with high porosity and permeability form the reservoir
54 bodies.

55 Within the oil industry the spatial distribution and geometry of the
56 reservoir bodies is commonly investigated (Jones et al., 1995; Willis and
57 Tang, 2010; Attar et al., 2015). The geometry and distribution control
58 the reservoir connectivity, which is the ratio of the volume of the largest
59 connected reservoir body over the sum of the volume of all reservoir bodies.
60 The connectivity is closely linked to the net-to-gross ratio (N/G), which is
61 the net reservoir volume versus the total volume (Hovadik and Larue, 2007).
62 Above 50% N/G the connectivity is more than 95% and it is unlikely that
63 this is a significant uncertainty (King, 1990). For fluvial reservoir systems the
64 connectivity is most sensitive between 10 and 20% N/G. The connectivity is
65 about 20% for reservoirs with N/G of 10% and it reaches 80% for reservoirs
66 of 20% N/G (Larue and Hovadik, 2006). This range in N/G is river type
67 dependent; for example, for rivers with high sinuosity the range shifts to
68 lower N/G values (Hovadik and Larue, 2007).

69 Larue and Hovadik (2008) studied the effect of N/G and connectivity
70 on oil recovery in a doublet system. For reservoirs with a connectivity
71 above 95%, they found that geological parameters such as sinuosity and
72 width/thickness ratio of the geo bodies and the orientation of the wells
73 compared to the geobodies have a relatively small effect on recovery and
74 water flooding efficiency. There is a small drop in oil recovery when the

75 N/G decreases from 50% to 20%. Below the 20% N/G the oil recovery drops
76 drastically from 80% to roughly 25% (Larue and Hovadik, 2008).

77 In the geothermal sector depositional processes and the building of various
78 sedimentological architectures are not commonly considered when the effect
79 of human controlled and physical parameters on the doublet performance is
80 investigated. Simplified geological representations are commonly used such
81 as homogeneous models (Saeid et al., 2014) or layer cake models (Poulsen
82 et al., 2015; Mottaghy et al., 2011; Deo et al., 2014). In the Netherlands
83 the software program ‘DoubletCalc’ is commonly used for prediction of the
84 doublet performance. This free software provided by TNO uses homogeneous
85 sand box models to calculate the obtained power of a low-enthalpy geothermal
86 doublet (Mijnlief et al., 2012), assuming that the connectivity and N/G are
87 both 100%. Studies in the oil-sector, however, show that these parameters
88 have a major impact on the fluid flow patterns (Hovadik and Larue, 2007) and
89 the recovery (Larue and Friedmann, 2005; Hovadik and Larue, 2007; Larue
90 and Hovadik, 2008). The lessons learnt in the oil industry sector provide some
91 insight on the importance of the use of detailed reservoir representations in
92 a geothermal system. These lessons however cannot be applied directly to
93 geothermal studies because oil is only extracted from the pore volume, while
94 the heat extracted from geothermal reservoirs is obtained from the fluid in
95 the pores and from the rock matrix.

96 In this paper process-based facies modelling is used to create realistic
97 representations of sedimentary reservoirs. Over 45 representations, called
98 reservoir realisations are created with a N/G ranging from 10 to 100%. A
99 finite element method (FEM) is utilised to simulate the fluid flow and heat

100 transfer processes in geothermal doublets. In the first part of this paper
101 the modelling approach is explained for both the generation of reservoir
102 realisations and the non-isothermal simulations. Next the relation between
103 N/G and the doublet performance parameters (life time and recovery) is
104 discussed, followed by the effect of the discharge rate. Then, the results
105 are combined to obtain a so-called ‘design model’, which estimates the life
106 time of a doublet and the recovery. In the end the difference between
107 randomly generated realisations and the reservoir realisations is assessed to
108 highlight the relevance of the facies based reservoir realisation in low-enthalpy
109 geothermal reservoir modelling.

110 **2. Methodology**

111 *2.1. Reservoir models*

112 This work consists of two main parts: static geomodels and dynamic
113 reservoir simulation. The static geomodels, with different N/G ranging from
114 10 to 100%, are generated in three different ways: Model Type I and II
115 are made utilising a process-based facies modelling approach to distribute
116 different facies Types (i.e. sand, shale); Model Type III is made using a
117 random facies field generator. The difference between Type I and II is the way
118 in which properties are assigned to the sand bodies. In Type I porosity and
119 permeability are heterogeneous within the sand bodies whereas in the Model
120 Type II single average porosity and permeability values are assigned for the
121 sand bodies. The realisations are then employed for conducting dynamic
122 simulations (Figure 1). The heat transfer in the reservoir and temperature
123 at the production well are calculated over time by using the software package

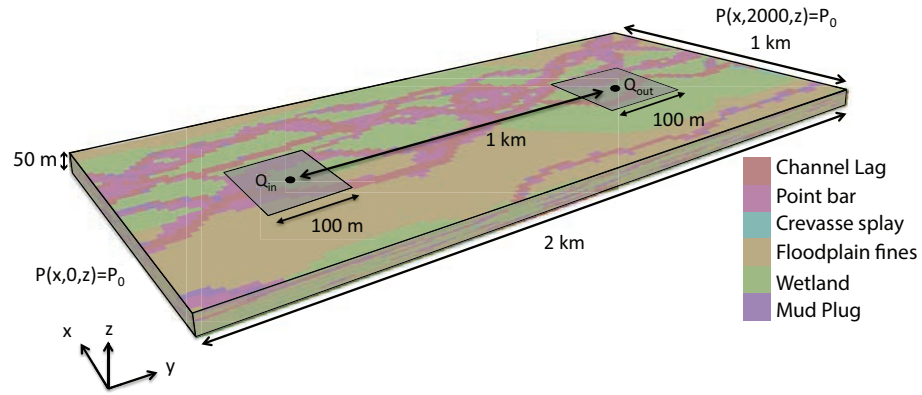


Figure 1: Schematic of the model domain and the well locations.

124 COMSOL Multiphysics utilising a finite element method. In the base case
 125 (initial) scenario the discharge is $100 \text{ m}^3/\text{h}$, the initial reservoir temperature is
 126 $75 \text{ }^\circ\text{C}$ and for the base case scenario the production stops when the production
 127 temperature drops to $74 \text{ }^\circ\text{C}$ (Minimal production temperature, T_{min}). The
 128 decline in the production temperature can be seen as the arrival time of the
 129 cold water front. Flow and heat transfer simulations are conducted employing
 130 all the generated reservoir realisations for several scenarios with different
 131 discharge rates ($80, 100, 120$ and $140 \text{ m}^3/\text{h}$). Consequently, the life time
 132 values and total heat recovery are calculated for different minimal production
 133 temperatures ($74, 72, 70$ and $68 \text{ }^\circ\text{C}$).

134 *2.1.1. Reservoir model Type I, II and III*

135 Process-based facies modelling software Flumy (Grappe et al., 2012) is
136 utilised to generate 48 realisations (depositional models) of a $1\text{km} \times 2\text{km} \times 50\text{m}$
137 geothermal reservoir with a resolution of $20\text{m} \times 20\text{m} \times 2.5\text{m}$. In this process-based
138 approach, facies are distributed mainly by modelling sedimentological processes.
139 Lopez et al. (2009) suggest that the constructed reservoir models utilising
140 a combined stochastic and process-based approach are realistic. This is
141 because the channels sizes and shapes are explicitly related to channel width,
142 channel depth, and avulsion frequency within other controlling parameters.
143 For example, the location of a fluvial channel after the avulsion depends on
144 the topography created by the previous flow path and deposition of sediment.
145 Note that while the constructed models are not conditioned by input data
146 such as logs or cores the geological data constrains range of the controlling
147 parameters in the process-based model. The method is explained in detail
148 in Grappe et al. (2012) and Lopez et al. (2009).

149 The resulting realisations contain seven Types of geobodies; pointbars,
150 sand plugs, channel lag, crevasse splays, levees, overbank floodplain fines and
151 mud plugs. The sedimentological processes depend on parameters such as
152 avulsion frequency, flood frequency, paleo-channel width and depth, maximum
153 floodplain deposit thickness and topography of the floodplain. In all of the
154 generated realisations the paleo flow, from the southeast to northwest is
155 oriented parallel to the long edge of the reservoir boundary (Figure 1). The
156 paleo-channel width and depth considered in this study are 40m and 4m,
157 respectively. These values and paleo-flow direction are derived from core
158 interpretations of the Lower Cretaceous Nieuwerkerk Formation in the West

Table 1: Reservoir sand body geometries. (*Donselaar and Overeem, 2008; Pranter et al., 2007**).

Bank-full flow width	40m*
Bank-full flow depth	4m
Meander belt width	800-1200m*
Single-story sandstone body thickness	4-5m
Single-story sandstone body width	200-400m*
Multi-story sandstone thickness	6-20m
Multi-story sandstone width	100-500
Width/thickness ratio sandstone bodies	16-100**

159 Netherlands Basin (DeVault and Jeremiah, 2002). The choice of orienting
 160 the paleo-flow direction parallel to the long-edge increases the connectivity
 161 in the reservoir realisations compared to a paleo flow perpendicular to the
 162 long edge. The ranges of process parameter values used for the modelling
 163 are derived from well core data and presented in Table 1 .

After the reservoir realisations are generated, the model is simplified by dividing the 7 types of geobodies into two groups; sand (channel lag, point bar, sand plug) and shale (crevasse splay, levee, overbank alluvium, mud plug). The sand group is considered as reservoir and the shale group as non-reservoir and the groups are used to calculate the N/G of the realisations. Sandstone grain size heterogeneity within sandstone bodies depends on paleo flow speed, and the proximity to the channel axis and river bends. As a result, the permeability of channel lags, point-bars and sand plugs varies across sandstone bodies (Willis and Tang, 2010). Therefore the heterogeneity of the

facies in the sand group is assumed to be captured by using the sandstone permeability distribution from the core measurements (TNO, 1977). A beta distribution correlation function was used to generate a heterogeneous porosity field within the sand group. The distribution characteristics including: mean, standard deviation, skew and kurtosis are equal to 0.28, 0.075, 0.35 and 2.3, respectively. The permeability of this group is derived from a porosity-permeability relationship obtained from petrophysical data of well MKP-11 (TNO, 1977):

$$\kappa = 0.0633e^{29.507\phi} \quad (1)$$

164 Where κ is the permeability [mD] and ϕ is the porosity [-]. The effect of
165 heterogeneity in the thermal rock properties on heat transfer in the geothermal
166 reservoir is insignificant compared to the heterogeneity in the flow properties
167 (Mottaghy et al., 2011). Therefore the thermal rock properties are considered
168 homogeneous and isotropic. The porosity and permeability of the shale group
169 are also assumed to be homogeneous and isotropic (Table 2).

170 To determine the effect of the heterogeneous porosity of the reservoir
171 bodies, some of the reservoir realisations are rebuilt with a homogeneous
172 sand group and named as model Type II. The porosity and permeability of
173 the sand group is equal to the averaged porosity and permeability of the sand
174 group in the reservoir realisations of model Type I. The size and distribution
175 of the reservoir bodies are kept the same.

176 Further, to study the relevance of process-based facies modelling on the
177 estimation of the life time and energy production of the doublets, geo-model
178 realisations (model Type III) are generated with the sand and shale facies
179 randomly (uncorrelated) distributed. The reservoir bodies have a constant
180 porosity of 28% and constant permeability of 1000 mD. All other parameters

181 are kept constant as in the model Type I. The differences in life time and
182 production between a processed-based facies reservoir model (Type I) and a
183 random realisation (Type III) are a measure of the importance of process-based
184 models used in geothermal reservoir simulations.

185 *2.2. Flow and heat transfer model*

186 The generated reservoir realisations (Type I, II and III) are employed for
187 heat transfer and fluid flow modelling. Figure 1 illustrates the reservoir and
188 the well locations (well spacing is 1 km). The injection and the production
189 wells have the same discharge rate which remains constant over time. The
190 two outer boundaries at the short edge are assigned a constant pressure, the
191 others are no flow boundaries (Figure 1). The N/G at the well positions,
192 in all dynamic models, has to be roughly the same as the N/G of the field,
193 especially for reservoir realisations with low N/G. In some of the reservoir
194 realisations the well may not be in contact with any sand body. This would
195 increase the well pressure and change the flow patterns within the realisation.
196 In this work, the maximum allowable difference between N/G at the wells
197 and the reservoir realisation is 2.5%. To achieve this the doublet can be
198 placed within a range of 50 m in the x and y direction from the original
199 well locations (Figure 1). The orientation of the doublet and the distance
200 between the wells are kept constant in all simulations.

201 *2.2.1. Governing equations*

202 Heat transfer in geothermal systems can be described with two main
203 processes: conduction and convection. For a system with a rigid rock,
204 incompressible fluids and local thermal equilibrium between rock and fluid

205 the heat transfer equation reads:

$$\frac{\partial}{\partial t}(\rho C T) = \nabla \cdot (\boldsymbol{\lambda} \nabla T) - \nabla \cdot (\rho_f C_f \mathbf{u} T) + \rho_f C_f q T^* \quad (2)$$

206 Where t is time [s], T the temperature [K], $\boldsymbol{\lambda}$ the total conductivity tensor
 207 [W/(kgK)], ρ_f the fluid density [kg/m³], C_f the fluid specific heat capacity
 208 [J/mK], \mathbf{u} Darcy velocity vector [m/s], and ρC is the volumetric heat capacity,
 209 q is external sinks and sources [1/s], and T^* refers to the temperature at
 210 sources. Darcy velocity is calculated as: $\mathbf{u} = -(\kappa/\mu)\nabla P$. Where μ is the
 211 dynamic viscosity [Pa.s] and P is the fluid pressure [Pa]. The fluid pressure
 212 field can be obtained by solving the continuity equation: $\phi \partial \rho_f / \partial t + \nabla \cdot$
 213 $(\rho_f \mathbf{u}) = \rho_f q$. The total thermal conductivity is expressed as: $\boldsymbol{\lambda} = \lambda_{eq} \mathbf{I} + \boldsymbol{\lambda}_{dis}$.
 214 Where λ_{eq} is the equivalent conductivity of the fluid and the matrix and
 215 the $\boldsymbol{\lambda}_{dis}$ the thermal dispersion tensor. This equivalent conductivity and the
 216 volumetric heat capacity are both volume averaged:

$$\begin{aligned} \lambda_{eq} &= (1 - \phi) \lambda_s + \phi \lambda_f \\ \rho C &= (1 - \phi) \rho_s C_s + \phi \rho_f C_f \end{aligned} \quad (3)$$

217 Where the suffixes s and f stand for solid (shale, sand) and fluid (brine),
 218 respectively.

219 Thermal dispersion has influence on the total conductivity. Thermal
 220 dispersion can be described as a function of the fluid velocity and fluid
 221 heat properties. The thermal dispersion tensor which is based on the solute
 222 dispersion model (Scheidegger, 1961), reads:

$$\boldsymbol{\lambda} = (\lambda_{eq} + (\alpha_T)|\mathbf{u}|)\mathbf{I} + \rho_f C_f (\alpha_L - \alpha_T) \frac{\mathbf{u}\mathbf{u}}{|\mathbf{u}|} \quad (4)$$

223 $|\mathbf{q}|$ is the magnitude of the Darcy velocity vector and α_L and α_T are the
 224 thermal dispersion coefficients in the longitudinal and transversal direction,
 225 respectively.

226 The pore fluid used in the dynamic model is brine. The brine has a
 227 constant specific heat capacity, heat conductivity and salinity (Table 2). The
 228 viscosity of the brine varies with temperature (T) and S the salinity of the
 229 brine [ppm/ 10^6] (Batzle and Wang, 1992) as:

$$\mu = 0.1 + 0.333S + (1.65 + 91.9S^3)e^{\{-[0.42(S^{0.8}-0.17)^2+0.045]T^{0.8}\}} \quad (5)$$

230 The density of the brine depends on the temperature, the pressure and
 231 the salinity as:

$$\begin{aligned} \rho_f = & \rho_w + S\{0.668 + 0.44S + 10^{-6}[300P - 2400PS \\ & + T(80 + 3T - 3300S^3P + 47PS)]\} \end{aligned} \quad (6)$$

Where

$$\begin{aligned} \rho_w = & 1 + 10^{-6}(-80T - 3.3T^2 + 0.00175T^3 + 489P - 2TP + 0.016T^2P \\ & - 1.3 * 10^{-5}T^3P - 0.333P^2 - 0.002TP^2) \end{aligned} \quad (7)$$

232 For equations 5 to 7, T is in [$^{\circ}\text{C}$] and P in [MPa] (Batzle and Wang, 1992).

233 The model domain is discretised by 3D tetrahedral and hexahedral finite
 234 elements. In general, discretization errors are the dominant sources of numerical

235 errors in simulations (e.g. Nick et al., 2009). To minimise the discretisation
236 error a maximum finite element mesh size of $20 \times 20 \times 2.5$ m is chosen. The
237 minimum finite element mesh size is 0.5 m. The maximum mesh size is
238 the same as the resolution of the geomodels. This avoids porosity and
239 permeability upscaling (averaging properties due to grid coarsening) of reservoir
240 realisations. Saeid et al. (2015) analysed the discretisation error for a similar
241 dynamic model and found that the chosen mesh size results in a negligible
242 discretisation error for the fluid and heat transfer simulations for the range of
243 studied parameters. In this study, the relative and absolute error tolerances
244 for flow and heat transport simulations are set to 10^{-5} and 10^{-6} , respectively.

245 *2.2.2. Life time*

246 The water temperature calculated at the production well is used to obtain
247 the life time of the doublet. The life time of the doublet is determined at
248 the time when the production fluid temperature drops below the minimal
249 production temperature. The temperature losses in the surface facilities and
250 the wells are neglected. Saeid et al. (2015) illustrated that the temperature
251 losses in the wells have negligible effect on the temperature of the production
252 fluid of a geothermal system.

253 *2.2.3. Recovery and Net energy production*

254 The calculated production temperature over time can be used to obtain
255 recovery, $R = E_{prod}/E_{total}$. Where R is the recovery of the field [%], E_{prod}
256 the cumulative produced energy [J] and E_{total} the total available energy [J].
257 The cumulative produced energy is defined as:

$$E_{prod} = \sum_{i=1}^n Q_i \Delta t_i \rho_f C_f (T_{prod,i} - T_{inj}), \quad (8)$$

258 and the total available energy as:

$$E_{total} = \sum_{j=1}^m \{V_j \phi_j \rho_{f,j} C_{f,j} (T_0 - T_{inj}) + V_j (1 - \phi_j) \rho_{s,j} C_{s,j} (T_0 - T_{inj})\} \quad (9)$$

259 Where Δt is the time step increment, the subscript i the time step, n total
 260 number of time steps, Q the discharge [m^3/s], $T_{prod,i}$ and T_{inj} the temperature
 261 [K] of the production fluid and the injection fluid at step i , respectively. m
 262 is the total number of finite elements, V_j the volume of the mesh element j
 263 and T_0 is the initial temperature [K].

264 The energy production is the produced energy minus the pump energy
 265 that is required to induce a pressure difference between the injection and the
 266 production well: $E_{net} = E_{prod} - E_{pump}$. Where E_{pump} is the required pump
 267 energy, assuming the efficiency of the pumps is equal to 1:

$$E_{pump} = \sum_{i=1}^n Q \Delta t_i (P_{inj} - P_{prod}) \quad (10)$$

268 3. Results

269 3.1. Base case

270 When applying the base case conditions for the dynamic simulation of
 271 different realisations of model Type I the following features were observed:
 272 (i) the N/G has noticeable impact on the life time of the doublet especially

Table 2: List of parameters used in the dynamic model.

Parameter	Description	Value	Dimension
α_L	Longitudinal dispersion coefficient	6.5	m
α_T	Transversal dispersion coefficient	2.2	m
κ_{shale}	Permeability of the shale bodies	5	mD
λ_f	Conductivity of the pore fluid	0.7	W/m/K
λ_{sand}	Conductivity of the sand bodies	2.7	W/m/K
λ_{shale}	Conductivity of the shale bodies	2.0	W/m/K
ρ_{sand}	Density of the sand bodies	2650	kg/m ³
ρ_{shale}	Density of the shale bodies	2600	kg/m ³
ϕ_{sand}	Average porosity of the sand bodies	0.28	-
ϕ_{shale}	Porosity of the shale bodies	0.1	-
C_f	Specific heat capacity of the pore fluid	4200	J/kg/K
C_{sand}	Specific heat capacity of the sand bodies	730	J/kg/K
C_{shale}	Specific heat capacity of the shale bodies	950	J/kg/K
L	Well spacing	1000	m
P_0	Initial pressure	200	bar
S	Salinity of the pore fluid	3	ppm/10 ⁶
T_0	Initial temperature	348	K
T_{inj}	Injection temperature	308	K

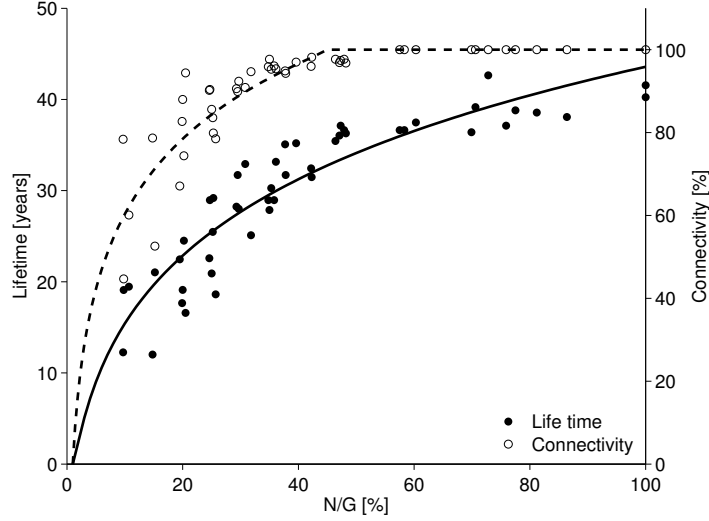


Figure 2: Life time of the doublet for $Q = 100 \text{ m}^3/\text{h}$ and $T_{min} = 74^\circ\text{C}$ and connectivity versus N/G, for model Type I realisations.

273 for low N/G values (Figure 2); (ii) decreasing N/G results in decreasing the
 274 life time, which is more pronounced for realisations with N/G smaller than
 275 40%; and (iii) the cumulative energy production shows the same results as the
 276 recovery (Figure 3), but the recovery increases slightly faster at N/G values
 277 larger than 60%. Since the differences between recovery and the cumulative
 278 energy production are negligible only the obtained recovery is discussed in
 279 this study. The recovery shows a similar relation with N/G as the life time
 280 (Figure 3). Note that 40% N/G is the point where the connectivity starts to
 281 decrease with lower N/G values.

282 Based on the obtained life time and recovery values for the base case
 283 scenario, the life time and recovery can be described as functions of N/G:

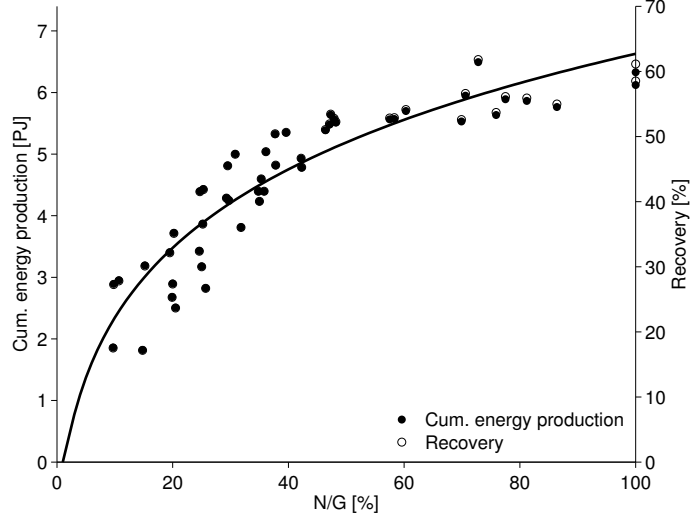


Figure 3: Total energy production and recovery versus N/G for $Q = 100 \text{ m}^3/\text{h}$ and $T_{min} = 74^\circ\text{C}$ utilising model Type I realisations.

$$LT = \alpha_{LT} \ln(N/G)^\gamma \quad (11)$$

and

$$R = \beta_R \ln(N/G)^\gamma \quad (12)$$

284 Where LT is the life time [years] and R the recovery [%]. α_{LT} and α_R are
 285 the fitting parameters for life time and recovery, respectively. For the base
 286 case scenario the fitting parameters α_{LT} , β_R and γ are equal to 4.41, 6.35
 287 and 1.5, respectively.

288 The variation in the temperature breakthrough curves obtained at the
 289 well production for reservoir realisations (Type I) with similar N/G values
 290 increase significantly with a decreasing N/G . For a N/G of around 50% the

291 breakthrough temperatures are almost identical (Figure 4-C). At a N/G
292 of around 30% the time at which the temperature starts to drop and the
293 gradient at which it drops start to differ among the realisations (Figure 4-B).
294 The differences are even larger at a N/G around 10% (Figure 4-A). The
295 variations can also be seen in the required energy for the pump (Figure 5).
296 A higher energy requirement means that more energy is needed to have the
297 same discharge implying that the sand bodies at the injection well are less
298 connected to the sand bodies at the production well. As a result the net
299 energy produced is less scattered than the total energy produced at very low
300 N/G.

301 The difference in the temperature breakthrough curves originates from the
302 difference in the corresponding medium configurations. Reservoir realisations
303 with a N/G of 10% in Figure 4-A illustrate that the location and geometry of
304 the sand bodies determine which part of the reservoir has a high permeability
305 zone. These geometries differ per realisation. Some sand bodies go straight,
306 while others are curved and/or split in two, which also results in isolated
307 sand bodies in different locations in the domain. When the N/G increases
308 this effect becomes less. At a N/G around 30% there are still some continuous
309 shale bodies separating the sands (Figure 4-B). The shales form low permeable
310 zones functioning as flow barriers. For realisations around 50% N/G, the sand
311 bodies are all connected to each other and cover the whole area, which makes
312 the realisations look more alike (Figure 4-C).

313 *3.2. Effect of discharge on geothermal doublet performance*

314 As expected, with increased discharge rates, the life time of the doublet
315 decreases (Figure 6). Similarly, with increased discharge, the variance in

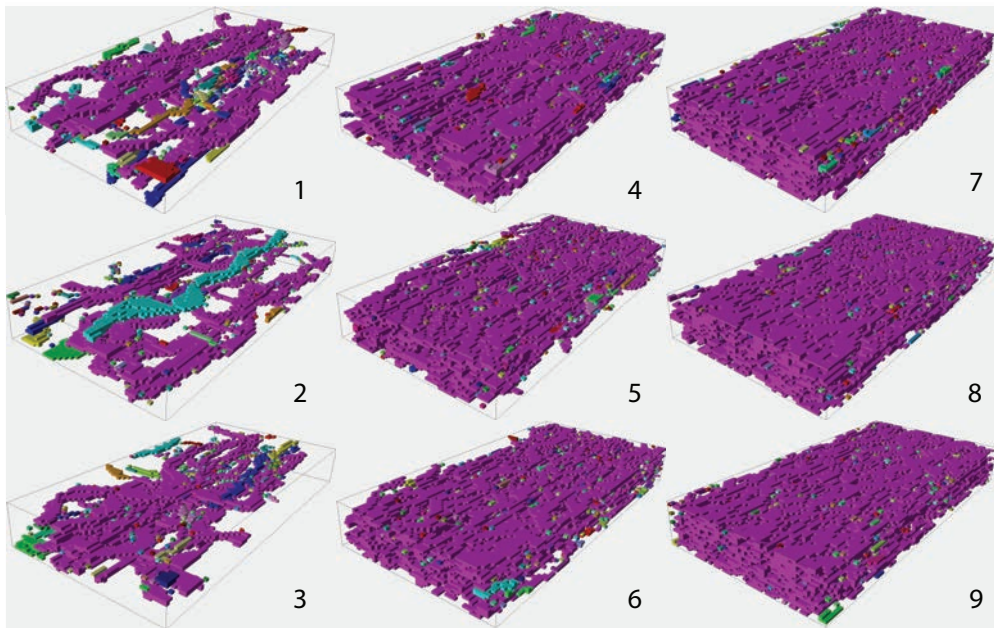
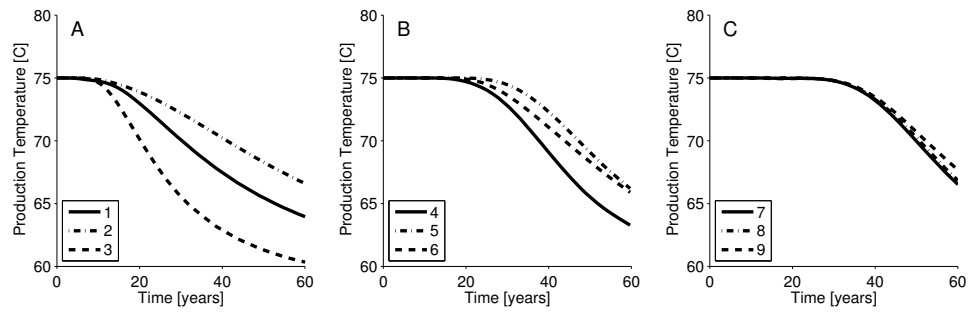


Figure 4: Production temperature development for $Q = 100 \text{ m}^3/\text{h}$, corresponding to different Type I realisations (1 to 9). Claystone gridblocks are transparent, and connected sandstone bodies have the same colour.

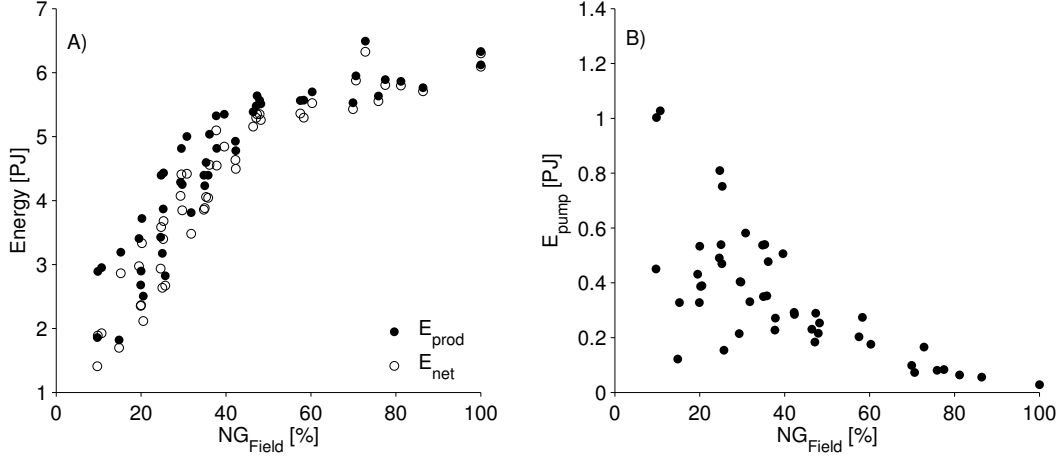


Figure 5: A) The produced energy and the net produced energy versus N/G. B) Pump energy required to create the pressure difference at the wells versus N/G (Eq. 10).

316 life time among realisations (Type I) is reduced (Figure 7). This is related
 317 to the fast decrease in life time for reservoirs with a large N/G. When the
 318 discharge rate goes from 60 to 100 m³/h, the life time decreases with ~20
 319 years for Type I realisations with a N/G of 100%, while at a N/G of 10% life
 320 time decreases with ~10 years. At high discharge rates ($Q > 200$ m³/h) an
 321 increase in the discharge has rather negligible effect on the life time, while
 322 at low discharge rates ($Q = 60$ m³/h) small changes have a large impact on
 323 the life time, 10 years difference compared with $Q = 80$ m³/h (Figure 7).

324 The type of relation between the N/G and life time does not change for
 325 different discharges, but it affects the fitting parameter α_{LT} . This fitting
 326 parameter has a linear relation with $1/Q$ (Figure 8-A):

$$\alpha_{LT} = \frac{\alpha_Q}{Q} \quad (13)$$

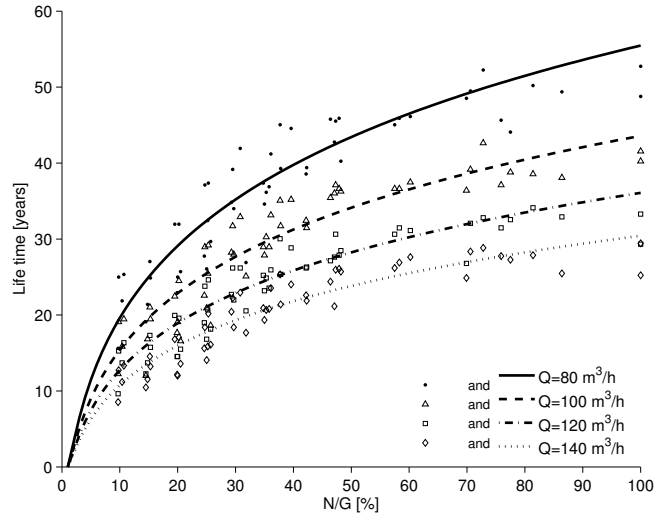


Figure 6: Life time versus N/G for different discharge rates ($T_{min} = 74^{\circ}\text{C}$).

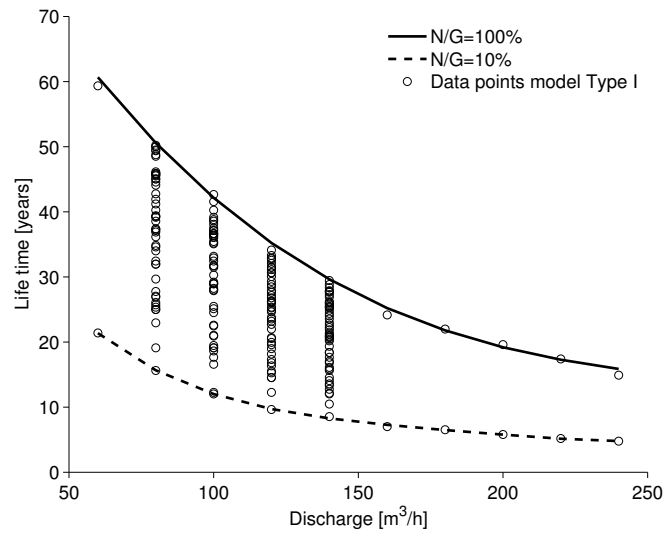


Figure 7: The variance in obtained life time values for N/G at different discharge rates and $T_{min} = 74^{\circ}\text{C}$

$$\beta_R = \frac{\beta_Q}{Q} \approx \text{constant} \quad (14)$$

327 Where α_Q is the discharge fitting parameter. The fitting parameter of the
 328 recovery, β_R , is barely sensitive to increasing $1/Q$ (Figure 8-B) and therefore
 329 the effect of discharge on β_R is neglected. Neither does the discharge variation
 330 have effect on the fitting parameter γ .

331 *3.3. Influence of the minimal production temperature on geothermal doublet*
 332 *life time and recovery*

333 A decrease in the minimal production temperature results in a longer life
 334 time and higher recovery (Figure 9). As a result the fitting parameters α_Q
 335 and β_R are specific for each production temperature. The lower the minimal
 336 production temperature the steeper the relation between parameters α_{LT} and
 337 $1/Q$ (Figure 8-C). The discharge fitting parameter α_Q has a linear relation
 338 with the temperature difference (Figure 8-A). As a result the complete curve
 339 for life time estimations becomes steeper, which gives an overestimation for
 340 reservoirs with a N/G above 60%. To correct for this overestimation the
 341 fitting parameters γ is defined as a function of ΔT :

$$\alpha_Q = 221\Delta T + 176 \quad (15)$$

$$\beta_R = 3.04\Delta T + 2.77 \quad (16)$$

$$\gamma = -0.115\Delta T + 1.585 \quad (17)$$

342 where $\Delta T = T_0 - T_{prod}$. Note that this relation is best suitable for ΔT
 343 up to 10 °C.

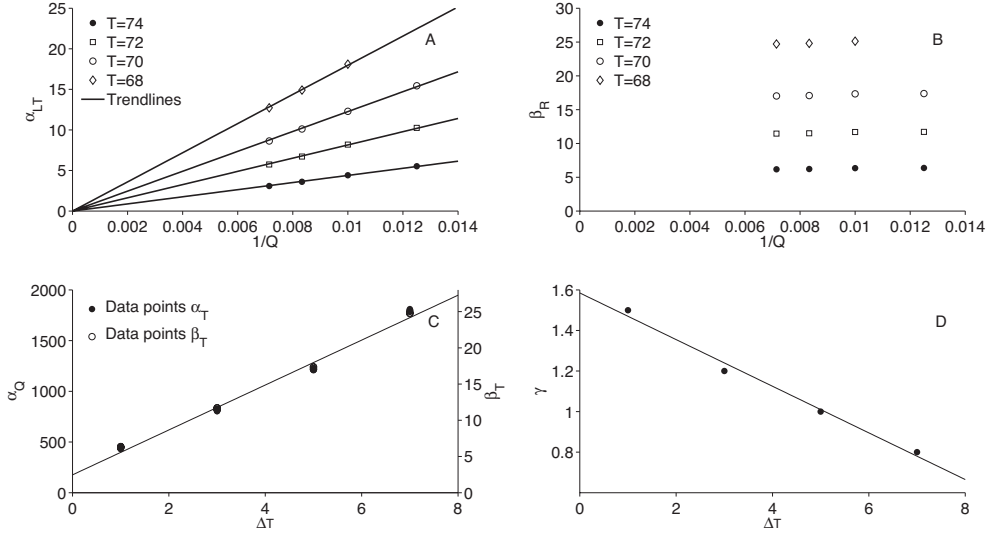


Figure 8: (A) α_{LT} versus $1/Q$ for different minimal production temperatures, (B) β_R versus $1/Q$ for different minimal production temperatures, (C) α_Q and β_T versus ΔT and (D) γ versus $1/Q$.

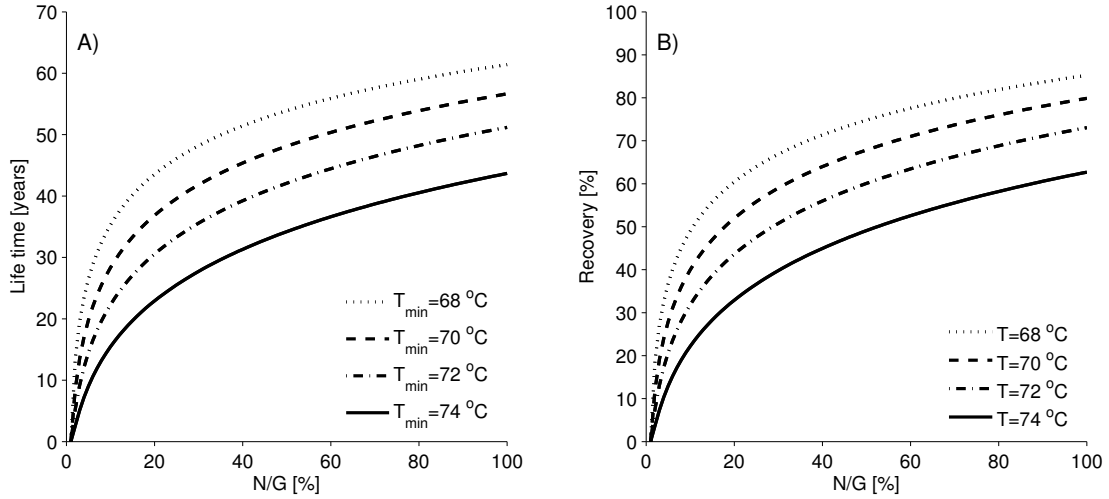


Figure 9: (A) The life time and (B) recovery versus N/G of model Type I realisations with a minimal production temperature of 68, 70, 72 and 74 °C for $Q = 100 \text{ m}^3/\text{h}$.

344 *3.4. Homogeneous versus heterogeneous reservoir bodies*

345 The reservoir realisations with homogeneous reservoir bodies (Type II)
346 have a slightly higher life time, 1.6 years on average with a maximum of 4.2
347 years, than that of model Type I realisations with heterogeneous reservoir
348 bodies (Figure 10). The overestimation falls mostly within the uncertainty
349 level of the calculated life times, which is related to the reservoir heterogeneity.

350 *3.5. Random realisations versus Reservoir realisations*

351 Utilising the random realisations (Type III) with N/G higher than 70%
352 results in life time values comparable to those calculated for the model Type
353 I realisations (Figure 11-A). Utilising model Type III realisations in the
354 dynamic model results in an overestimation of the life time for N/G values
355 between 70% to 40%, where the life time is almost stable. Below 40% N/G
356 the life time starts to drop in case of Type III realisations, but less than that
357 of the Type I realisations. It is found that the connectivity values of the
358 reservoir for Type III realisations drops drastically and reaches zero for Type
359 III realisations with N/G less than 30%, while the Type I realisations have
360 a minimum connectivity of 42% (Figure 11-B). This means that the random
361 realisations (Type III) have reservoir bodies at the wells which are small and
362 isolated. These realisations do not have a high permeable zone between the
363 wells. And with respect to the boundary conditions, fixed discharge, the
364 pressure difference between the injector and producer increases significantly.
365 The models with the random realisations (Type III) result in a much lower
366 variance in life time for reservoirs with the same N/G value when they are
367 compared to the life time values obtained for the model Type I realisations
368 (Figure 11).

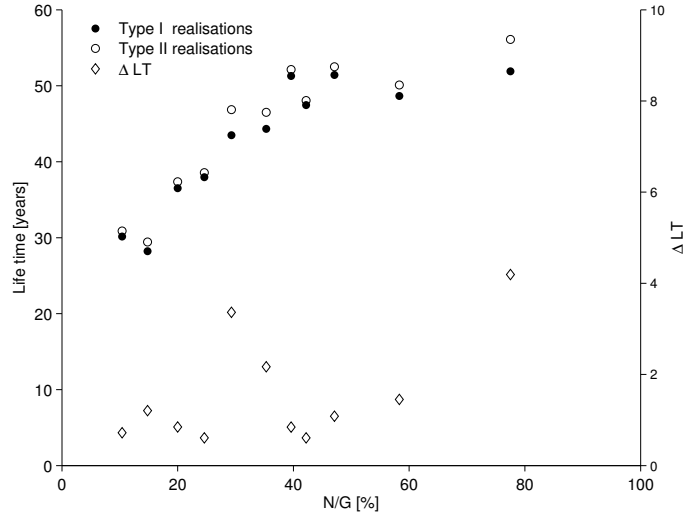


Figure 10: Life time versus N/G for reservoir realisations with heterogeneous (Type I) and homogeneous (Type II) sand bodies including the difference in life time between them (ΔLT) with $Q = 100 \text{ m}^3/\text{h}$ and $T_{min} = 74^\circ\text{C}$.

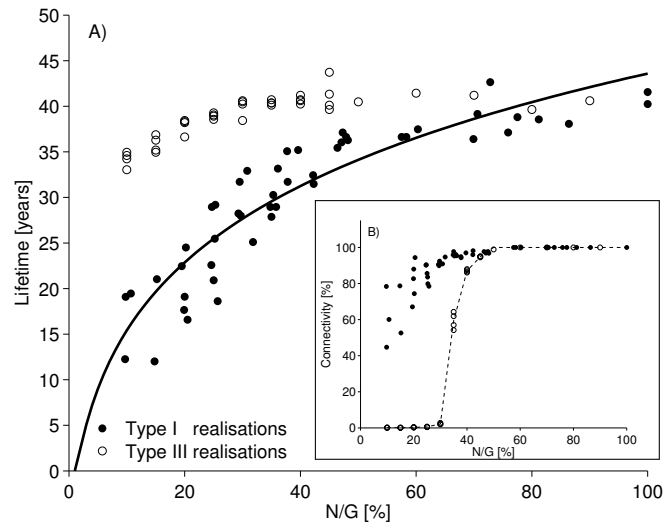


Figure 11: Life time versus the N/G of random realisation (Type III) and geological realisation (Type I) with $Q = 100 \text{ m}^3/\text{h}$ and $T_{min} = 74^\circ\text{C}$.

369 *3.6. A simple design model*

370 With respect to the results gained by employing the reservoir realisations
371 Type I, the life time of a reservoir can be estimated with a simplified model
372 when the N/G, discharge and minimal production temperature are known.
373 The model is described as:

$$LT = \frac{221\Delta T + 176}{Q} (\ln(N/G))^{(-0.115\Delta T + 1.585)} \quad (18)$$

$$R = (3.04\Delta T + 2.77) (\ln(N/G))^{(-0.115\Delta T + 1.585)} \quad (19)$$

374 The model is only tested for discharge rates between 80 and 140 m³/h and
375 minimal production temperature values down to 68 °C. More research needs
376 to be done to check if the model is valid for higher discharge values. The
377 linear relation of ΔT and life time is found not to be valid for all temperature
378 values. This is because below 65 °C the production temperature curve is no
379 longer linear (Figure 4), which indicates that the effect of ΔT on the life time
380 is non-linear.

381 The results obtained with the simplified model are comparable with the
382 results calculated with the dynamic model (Figure 12). The predicted life
383 time values are not exactly the same as those obtained from the dynamic
384 model. This is partly a result of the variance in life time of reservoir models
385 with similar N/G values (Figure 11). The effect is found to be the same for
386 the recovery.

387 *3.7. An improved design model*

388 The simplified model works fine, but it underestimates the life time for
389 discharges of 80 and 100 m³/h with a minimal temperature of 74°C. The

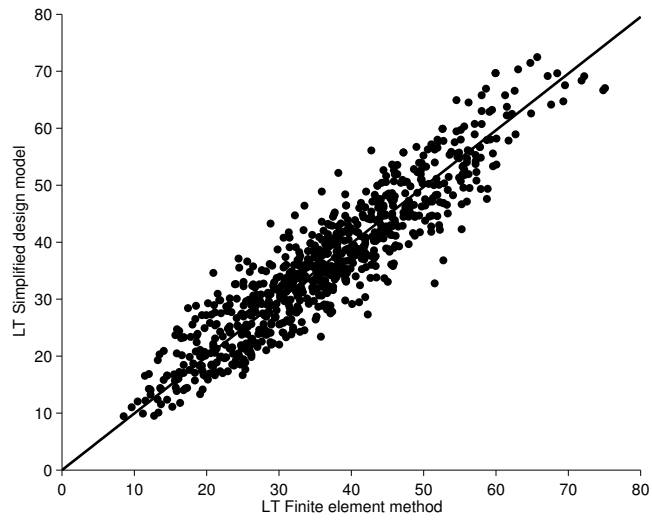


Figure 12: The life time calculated with the dynamic model versus the life time estimated with the simplified design model ($R^2 = 0.85$). The data points of all heat transfer and flow simulations of Type I are used.

390 model also overestimates the life time for reservoir realisation with a N/G
391 above 70% with a minimal production temperature of 70 and 68°C. This can
392 be improved by splitting the model up into 2 regions. Region 1 has a N/G
393 range from 10 to 45% and Region 2 from 45 to 100% N/G. In Region 1 a
394 similar function is used as in the simplified model, but fitting parameters are
395 adjusted to this region (Figure 13). The function is less complex, because
396 the fitting parameter γ is constant. In Region 2 the function is no longer
397 logarithmic, but linear. The improved design model is described as:

$$LT = \begin{cases} \frac{390+56.9\Delta T}{Q} (\ln(N/G))^{1.5} & \text{for } 15 < N/G \leq 45 \\ \frac{390+56.9\Delta T}{Q} (\ln(45))^{1.5} + \frac{18.7-2.84\Delta T}{Q} (N/G - 45) & \text{for } 45 < N/G < 100 \end{cases} \quad (20)$$

$$R = \begin{cases} (0.75\Delta T + 5.67)(\ln(N/G))^{1.5} & \text{for } 15 < N/G \leq 45 \\ (0.75\Delta T + 5.67)(\ln(45))^{1.5} \\ + (0.28 - 0.035\Delta T)(N/G - 45) & \text{for } 45 < N/G < 100 \end{cases} \quad (21)$$

398 This model describes the life time as a function of N/G, Q and ΔT , and
399 the recovery as a function of only N/G and ΔT . A clear distinction can
400 be made between the two regions. In Region 1 the geological parameter
401 N/G is the main controlling factor on both life time and recovery. The
402 human controlled parameter Q (discharge rate) is the most influential factor
403 in Region 2 on life time, while the human controlled parameter ΔT is the
404 most influential factor on the recovery.

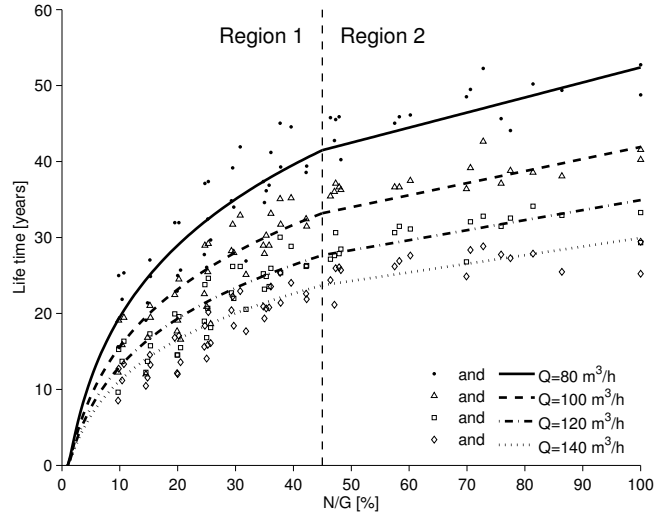


Figure 13: Life time versus N/G for different discharges based on the improved design model.

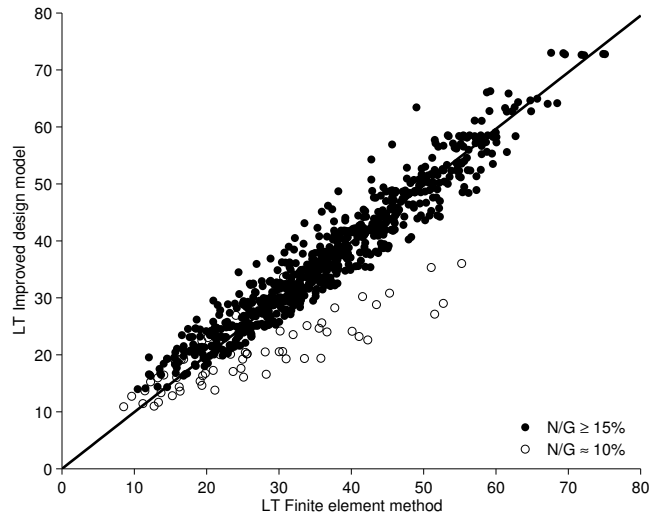


Figure 14: Life time obtained with the dynamic model versus the life time obtained with the improved design model ($R^2 = 0.92$). The data points of all heat transfer and flow simulations of Type I are used.

405 The improved design model predicts the life time more accurately compared
406 to the simplified design model; it improves R^2 from 0.85 to 0.92 (Figures 12
407 and 14). The improved design model works best for N/G from 15 to 100%,
408 but underestimates the life time of reservoirs with a N/G around 10% (Figure
409 14).

410 **4. Discussion**

411 *4.1. Base case - model Type I*

412 The effect of N/G on life time and recovery can be described with natural
413 logarithmic relations for N/G values below 45% and with linear relations for
414 N/G values above 45%. In Region 1 the connectivity has a larger variance,
415 precluding accurate prediction of the life time and recovery. The variance in
416 connectivity increases with decreasing N/G. This could partly be an effect
417 of the chosen resolution of the reservoir realisations (Type I), which result
418 in less accurate connectivity calculations for a N/G below 20%. Hovadik
419 and Larue (2007) showed that increasing the geomodel resolution decreases
420 variance for connectivity and improves connectivity. This in combination
421 with the effect of the facies distribution explains why it is harder to predict
422 doublet performances of low N/G reservoirs; more variables play a role. For
423 the linear part the relations are more accurate. The connectivity is 100% for
424 all realisations and has therefore negligible effect on the results.

425 The higher variance in life time for low N/G reservoirs indicates that the
426 accuracy of the reservoir model is crucial, which is for high N/G reservoirs
427 with lower variances less important, albeit not negligible. The energy recovery
428 shows the same effect as in the oil recovery; once the connectivity starts

429 to drop the recovery drops fast (Larue and Hovadik, 2008). The absolute
430 values of the recoveries from oil and geothermal energy can not be compared
431 directly, because the recoveries are defined in a different way. In the oil
432 industry the total amount of oil available is only in the pore of the reservoir
433 bodies, while the total amount of heat available is in the connected pores and
434 the matrix of both the reservoir and non-reservoir. This means the oil can
435 only be produced from the reservoir part, while heat can be produced from
436 the surrounding low permeable layers by conduction. Nonetheless, the heat
437 recoveries obtained in this study have a range from 15 to 65% (Figure 3),
438 which is similar to the oil recoveries reported by Larue and Hovadik (2008).
439 The differences between obtained energy recoveries for realisations with 50
440 and 100% N/G are small, which indicates that the shales play an important
441 role in geothermal doublet performance for reservoirs with N/G lower than
442 50%. As a result, reservoirs with a N/G of roughly 50% are almost as efficient
443 as those with 100% N/G. Notice that the heat capacity and conductivity are
444 similar for sand and shale, which makes the differences in heat conduction
445 small.

446 *4.1.1. Case A: Discharge*

447 Discharge affects the life time and recovery, but the difference in recovery
448 between a discharge of 80 and 140 m³/h is small compared to the variance in
449 recovery for reservoir simulations with similar N/G (Figure 3). This means
450 the discharge rate can be adjusted to the yearly energy demand, without
451 influencing the cumulative produced energy significantly during the life time
452 of the doublet.

453 The pressure in the injection well increases with increasing discharge or

454 when the well is only in contact with small isolated sand bodies. This pressure
455 can not be higher than the rock strength, otherwise the reservoir will be
456 fractured. Fractures in the reservoir would change the fluid flow behaviour
457 significantly (e.g. Matthäi et al., 2010; Nick et al., 2011) and the stated
458 relations would not be applicable.

459 *4.1.2. Case B: Minimal production temperature*

460 Lower minimal production temperatures extend the life time and recovery.
461 When the produced temperature declines the daily energy produced declines
462 as well, because the discharge is constant. If a constant daily energy production
463 is preferred the discharge has to increase to compensate for the produced
464 water with lower temperatures. This will decrease the life time of the project
465 and speed up the cooling of the production temperature. This loop will
466 accelerate the whole process and the differences in life time will be less than
467 shown in Figure 9-A.

468 The variance in the obtained life time and recovery increases for decreasing
469 minimal production temperatures (Figure 4). This is related to the dispersion
470 effect. The result of this effect is most noticeable after the cold water front has
471 reached the production well. The temperature of the produced water drops
472 more slowly for a system with higher thermal dispersion. This uncertainty
473 in temperature drop makes it harder to predict the life time and recovery for
474 lower minimal production temperatures.

475 *4.2. Homogeneous sand bodies - model Type II*

476 Reservoir realisations with homogeneous reservoir bodies may overestimate
477 the life time up to 4 years compared to reservoir realisations (Type I) with

478 heterogeneous sands, but in most cases the overestimation is less than 1
479 year. The difference in life time between homogeneous and heterogeneous
480 sands is within their uncertainty bounds. Therefore the intra sand-body
481 heterogeneity could be disregarded for the life time calculation.

482 *4.3. Random realisations - model Type III*

483 The simulations with the random realisation result in unrealistic required
484 (well) pressure values and in much higher life times compared to reservoir
485 realisations (Type I) when N/G values are below 70%. These unrealistic
486 pressure values are related to the fixed discharge rate and the shape and
487 connectivity of the reservoir bodies. Random porosity and permeability
488 fields hardly any random realisation has a connected reservoir body from
489 the injection to the production well, whereas the reservoir realisations do
490 have this. As a result very high injection well pressure values are needed to
491 push the water through the shale in between the sands in order to achieve
492 the required discharge rate.

493 A realistic geological model is therefore necessary for N/G values below
494 40%. Above 40% N/G the connectivity plays only a small role, as it is always
495 larger than 95%. The life time values obtained with the random realisations
496 are overestimated for a N/G between 40 and 60%. For N/G values above
497 70%, the life time obtained by the random realisations are comparable with
498 the ones obtained with reservoir realisations. Nevertheless, in the random
499 realisations the difference between maximum and minimum possible life times
500 is maximum 5 years, while the results of the reservoir realisation show that
501 the difference can be significantly larger (± 10 years), which seems to be the
502 case even for reservoirs up to 70% N/G (Figure 11-A). Therefore dynamic

503 reservoir simulations should be employed to calculate the risks of an early
504 cold water breakthrough, especially before drilling.

505 Even though it is hard to make very accurate reservoir simulations before
506 drilling, simulation results will provide a valuable range of expected life times.
507 This means that the geology has a major impact on life time and is as
508 important as the human controlled parameter ‘discharge’ when estimating
509 the life time of a low-enthalpy geothermal doublet.

510 When layer cake models are used to calculate the life time one major
511 assumption is that all the reservoir bodies are concentrated (i.e. 100%
512 connectivity). The comparison of the random realisations with reservoir
513 realisations shows that it is important to know the connectivity of the reservoir
514 body between the injection and production well, not only for the life time,
515 but for well pressure too. This means that if the injector is poorly connected
516 to the producer, higher pressures are needed to keep up the discharge. This
517 pressure varies the most for realisation below 45% N/G, which is the region
518 where the connectivity varies (Figure 2). The pressure increases are probably
519 less noticeable when layer cake models are used.

520 *4.4. Simplified and Improved design model*

521 The simplified model provides a good estimate of the life time of doublets
522 producing from low-enthalpy geothermal reservoirs. The model is only directly
523 applicable for reservoir with roughly the same heat transfer and flow characteristics,
524 well spacing and reservoir thickness as used in this study. The model assumes
525 that all reservoirs have the same type of non-linear relation, but the fitting
526 parameters are formation specific. Despite the limitations, the simplified
527 design model can be used for primary calculations for estimating life time and

528 recovery. It must be kept in mind, however, that the results underestimate
529 reality for the lower range of N/G between 35 and 50% and overestimate it
530 for a N/G above 90% (Figure 2). For the other values of N/G, the simplified
531 model gives a good average value, when the variance in life time and recovery
532 are taken into account.

533 The improved model estimates the life time more accurate than the
534 simplified model by dividing the model into 2 regions: a logarithmic part
535 and a linear part. This resolves the problem for the underestimations and
536 overestimations of the simplified model and removes the fitting parameter γ
537 from the equation. The decreasing accuracy of the simplified model due to
538 an increasing variance in life time remains the same in the improved model.
539 The variance combined with an underestimation at a N/G of 10% makes the
540 improved model less accurate for reservoirs with a N/G below 15%. This is,
541 however, no problem for the targets for low-enthalpy geothermal reservoirs in
542 the Netherlands, since the Nieuwerkerk Formation has a N/G between 20 and
543 50% (Den Hartog Jager, 1996). When applying the improved model to this
544 formation the calculated life time can still be between 21 years (N/G=20%)
545 and 31 years (N/G=31%) for Q equal to 100 m³/hr and ΔT equal to 1°C.
546 Inclusion of N/G values measured in nearby fields in the study area can
547 help narrowing this range of N/G and improving the life time prediction.
548 Nevertheless this implies that accurate field data and reservoir realisations
549 are necessary for accurate prediction of the doublets life time and recovery.

550 **5. Conclusions**

551 The work combines a process-based model with a flow and heat transfer
552 model. The process-based model is capable of generating reservoir models
553 (Type I and II) utilising core data. We show that the life time can be
554 estimated with the design model for both Region 1 ($N/G > 45\%$) and Region
555 2 ($N/G < 45\%$). We have demonstrated that the difference in life time within
556 Region 2 is relatively small and the main controlling factor is the discharge.
557 In Region 1 the dependence of life time on N/G is larger than in Region 2.
558 Therefore small over- and underestimation in N/G have a large impact on
559 life time predictions in Region 1. The shale has a positive contribution to
560 the heat transfer in the system, which increases the potential of lower N/G
561 reservoirs.

562 When using a geological model with randomly distributed facies, first the
563 life times are overestimated, especially for reservoirs in Region 1. Next, the
564 variance in life time for reservoirs with the same N/G is less than 5 years
565 for model Type III reservoirs, while it is 10 years when process-based facies
566 modelling (Type I) is used. This means a realistic representation of the facies
567 heterogeneity is needed to make more reliable predictions of the life time of
568 a low-enthalpy geothermal doublet.

569 **References**

570 **References**

- 571 Attar, A., Muggeridge, A., et al. (2015). Impact of geological heterogeneity on performance
572 of secondary and tertiary low salinity water injection. In *SPE Middle East Oil & Gas*
573 *Show and Conference*. Society of Petroleum Engineers.
- 574 Batzle, M. and Wang, Z. (1992). Seismic properties of pore fluids. *Geophysics*,
575 57(11):1396–1408.
- 576 Bonté, D., Van Wees, J.-D., and Verweij, J. (2012). Subsurface temperature of the
577 onshore netherlands: new temperature dataset and modelling. *Netherlands Journal*
578 *of Geosciences*, 91(04):491–515.
- 579 Den Hartog Jager, D. (1996). Fluvio-marine sequences in the lower cretaceous of the west
580 netherlands basin: correlation and seismic expression. In *Geology of gas and oil under*
581 *the Netherlands*, pages 229–241. Springer.
- 582 Deo, M., Roehner, R., Allis, R., and Moore, J. (2014). Modeling of geothermal energy
583 production from stratigraphic reservoirs in the great basin. *Geothermics*, 51:38–45.
- 584 DeVault, B. and Jeremiah, J. (2002). Tectonostratigraphy of the nieuwerkerk formation
585 (delfland subgroup), west netherlands basin. *AAPG bulletin*, 86(10).
- 586 Donselaar, M. E. and Overeem, I. (2008). Connectivity of fluvial point-bar deposits:
587 An example from the miocene huesca fluvial fan, ebro basin, spain. *AAPG bulletin*,
588 92(9):1109–1129.
- 589 Grappe, B., Cojan, I., Flipo, N., Riviorard, J., and Vilmin, L. (2012). Developments in
590 dynamic modelling of meandering fluvial systems. *AAPG Congres.*
- 591 Hovadik, J. M. and Larue, D. K. (2007). Static characterizations of reservoirs: refining
592 the concepts of connectivity and continuity. *Petroleum Geoscience*, 13(3):195–211.
- 593 Jones, A., Doyle, J., Jacobsen, T., and Kjønsvik, D. (1995). Which sub-seismic
594 heterogeneities influence waterflood performance? a case study of a low net-to-gross
595 fluvial reservoir. *Geological Society, London, Special Publications*, 84(1):5–18.
- 596 King, P. (1990). The connectivity and conductivity of overlapping sand bodies. *North Sea*
597 *Oil and Gas Reservoirs*, 2:353–362.
- 598 Larue, D. and Friedmann, F. (2005). The controversy concerning stratigraphic architecture
599 of channelized reservoirs and recovery by waterflooding. *Petroleum Geoscience*,
600 11(2):131–146.
- 601 Larue, D. and Hovadik, J. (2008). Why is reservoir architecture an insignificant uncertainty
602 in many appraisal and development studies of clastic channelized reservoirs? *Journal*
603 *of Petroleum Geology*, 31(4):337–366.

- 604 Larue, D. K. and Hovadik, J. (2006). Connectivity of channelized reservoirs: a modelling
605 approach. *Petroleum Geoscience*, 12(4):291–308.
- 606 Lopez, S., Cojan, I., Rivoirard, J., and Galli, A. (2009). Process-based stochastic
607 modelling: meandering channelized reservoirs. *Analogue Numer Model Sediment Syst:
608 From Understand Predict (Special Publ. 40 of the IAS)*, 40.
- 609 Matthäi, S. K., Nick, H. M., Pain, C., and Neuweiler, I. (2010). Simulation of solute
610 transport through fractured rock: a higher-order accurate finite-element finite-volume
611 method permitting large time steps. *Transport in porous media*, 83(2):289–318.
- 612 Mijnlief, H., Obdam, A., Kronimus, A., van Wees, J., van Hooff, P., Pluymaekers, M., and
613 Veldkamp, J. (2012). *Doubletcalc 1.4 Handleiding*. TNO, 1.4 edition.
- 614 Mottaghy, D., Pechnig, R., and Vogt, C. (2011). The geothermal project den haag: 3d
615 numerical models for temperature prediction and reservoir simulation. *Geothermics*,
616 40(3):199–210.
- 617 Nick, H., Paluszny, A., Blunt, M., and Matthai, S. (2011). Role of geomechanically
618 grown fractures on dispersive transport in heterogeneous geological formations. *Physical
619 Review E*, 84(5):056301.
- 620 Nick, H., Schotting, R., Gutierrez-Neri, M., and Johannsen, K. (2009). Modeling
621 transverse dispersion and variable density flow in porous media. *Transport in porous
622 media*, 78(1):11–35.
- 623 Poulsen, S., Balling, N., and Nielsen, S. (2015). A parametric study of the thermal recharge
624 of low enthalpy geothermal reservoirs. *Geothermics*, 53(0):464 – 478.
- 625 Pranter, M. J., Ellison, A. I., Cole, R. D., and Patterson, P. E. (2007). Analysis and
626 modeling of intermediate-scale reservoir heterogeneity based on a fluvial point-bar
627 outcrop analog, williams fork formation, piceance basin, colorado. *AAPG bulletin*,
628 91(7):1025–1051.
- 629 Saeid, S., Al-Khoury, R., Nick, H. M., and Barends, F. (2014). Experimental&numerical
630 study of heat flow in deep low-enthalpy geothermal conditions. *Renewable Energy*,
631 62(0):716 – 730.
- 632 Saeid, S., Al-Khoury, R., Nick, H. M., and Hicks, M. A. (2015). A prototype design model
633 for deep low-enthalpy hydrothermal systems. *Renewable Energy*, 77(0):408 – 422.
- 634 Scheidegger, A. (1961). General theory of dispersion in porous media. *Journal of
635 Geophysical Research*, 66(10):3273–3278.
- 636 TNO (1977). Nl olie- en gasportaal, www.nlog.nl.
- 637 van Heekeren, V., editor (2015). *The Netherlands country update on geothermal energy*,
638 Stichting Platform Geothermie. World Geothermal Congress.

639 Willis, B. J. and Tang, H. (2010). Three-dimensional connectivity of point-bar deposits.
640 *Journal of Sedimentary Research*, 80(5):440–454.